Alcohol Drinking Alters Stress Coping via Extended Amygdala Kappa Opioid Receptor Signaling in Male Mice

Authors: Lara S. Hwa, Sofia Neira, Meghan E. Flanigan, Christina M. Stanhope, Melanie M. Pina, Dipanwita Pati, Olivia J. Hon, Waylin Yu, Emily Kokush, Rachel Calloway, Kristen Boyt, Thomas L. Kash*

Affiliations: Bowles Center for Alcohol Studies, Department of Pharmacology, University of North Carolina at Chapel Hill, 104 Manning Drive, Chapel Hill, NC, 27599, USA

*Correspondence

Thomas L. Kash, Ph.D.

John R. Andrews Distinguished Professor

Bowles Center for Alcohol Studies

Department of Pharmacology

University of North Carolina School of Medicine

Chapel Hill, NC 27599, USA

tkash@email.unc.edu

(919)843-7867

Abstract

Maladaptive responses to stress are a hallmark of alcohol use disorder, but the mechanisms that underlie this are not well characterized. Here we show that kappa opioid receptor (KOR) signaling in the bed nucleus of the stria terminalis (BNST) is a critical molecular substrate disrupting stress-coping behavior following heavy alcohol drinking. Altered responses to an innate stressor were associated with enhanced PFC-driven excitation of prodynorphin-containing neurons in the BNST during protracted withdrawal from intermittent alcohol drinking. These findings suggest that increased corticolimbic connectivity may underlie impaired stress-coping during protracted withdrawal from heavy drinking and represents a target of potential therapeutic mediation as well as a potential biomarker of negative outcomes.

Impact Statement: Heavy alcohol drinking primes dynorphin / kappa opioid systems in the bed nucleus of the stria terminalis to alter stress coping responses.

Competing Interests: Authors declare no competing interests.

Data and materials availability: All data are available in the main text or the supplementary materials.

Introduction

Alcohol abuse exacts a tremendous toll on society. One key issue in alcohol abuse is that long term alcohol drinking can dysregulate stress systems in the brain. Prolonged alcohol drinking and withdrawal experiences result in enhanced responsiveness and behavioral sensitivity to stress during protracted abstinence (Heilig et al. 2010). Reciprocally, clinical studies show that negative stress coping is predictive of higher levels of drinking in alcoholics (Noone et al. 1999). Blunted responses to stress have been identified in alcohol-dependent people (Sinha et al. 2011), so it is essential to consider mechanisms by which alcohol drinking results in maladaptive stress responses during protracted abstinence. While many studies have utilized animal models to investigate how stress drives increased alcohol drinking behaviors (Becker et al. 2011, Gilpin and Weiner 2017), few have explored the effects of alcohol drinking on subsequent stress responsivity.

Chronic alcohol exposure engages brain stress signaling systems that influence drinking behaviors in a dynamic and complex manner (Koob and Kreek 2007). One such stress system is the neuropeptide prodynorphin (Pdyn) and its receptor, the kappa opioid receptor (KOR), which has been studied in the contexts of both mood and alcohol use disorders (Lutz and Kieffer 2013). Limbic structures implicated in alcohol and stress behaviors, such as the bed nucleus of the stria terminalis (BNST), are rich in Pdyn and KOR (Le Merrer et al. 2009). The BNST is an integrative hub that may mediate the negative affective state associated with chronic alcohol use (Koob 2009, Kash 2012). KORs throughout the extended amygdala and the BNST alter anxiety-like behavior in mice (Bruchas et al. 2009; Crowley et al. 2016) and mediate stress-induced reinstatement for alcohol reinforcement (Lê et al. 2018).

In this study, we tested whether BNST KOR/Pdyn signaling regulates maladaptive stress reactions after long-term alcohol drinking. We focused on stress reactions to the ethologically relevant predator odor trimethylthiazoline (TMT), a compound isolated from fox feces. In rats and C57BL/6J mice, TMT activates specific brain regions involved in stress, anxiety, and fear, including the BNST (Day et al. 2004, Asok et al. 2013, Janitzky et al. 2015), and inactivation of the BNST blocks TMT-induced freezing (Fendt et al. 2003). Recent work suggests that distinct neuropeptide circuits in the BNST may drive opposing emotional states (Giardino et al. 2018), which may be dependent on inputs from cortical sites to affect stress coping behaviors (Johnson et al. 2019). The current series of experiments integrate Pdyn-specific cell types and KOR signaling in the BNST as a neuromodulator of alcohol-drinking impaired behavioral responses to TMT. We show that KOR dysregulation of corticolimbic circuits underlies lasting behavioral changes to stressors that emerge after chronic drinking. This is a critical area of study, as mitigating stress responses can contribute to improved alcohol relapse outcomes.

Results

Male C57BL/6J mice were given six weeks of intermittent access to alcohol (EtOH), a protocol known to induce heavy voluntary drinking (Hwa et al. 2011), before behavioral testing both during early (<24 hr) and protracted (7-10 days) abstinence [Fig 1A, Fig 1 Suppl 1A]. Mice consumed high amounts of EtOH and increased their EtOH preference over time [Fig 1B]. During early abstinence, we found stress deficits in both the repeated forced swim test (Anderson et al. 2016, Commons et al. 2017) [Fig 1 Suppl 1B] and homecage predator odor TMT exposure (Hwa et al. 2019) [Fig 1 Suppl 1D-G]; however, only responses to the predator odor remain altered throughout protracted abstinence. Specifically, EtOH-drinking mice did not avoid the

TMT compared to the water (H_2O)-drinking controls during protracted abstinence [Fig 1C], suggestive of maladaptive survival behavior. Previous studies have shown that activation of the Pdyn/KOR system can modulate stress-induced EtOH seeking (Lê et al. 2018), so we tested if KOR blockade could alter drinking-induced stress behavior. Systemic treatment with 5 mg/kg of the long-acting KOR antagonist norBNI rescued the EtOH-induced impairment of predator odor response [Fig 1D-F]. Given the potential relevance of targeting the protracted time point, rather than at acute abstinence [Fig 1 Suppl 1A-G], we next focused on identifying the mechanism for this long-lasting adaptation.

The BNST is a brain site known for its involvement in stress, anxiety, and addiction, and is regulated by the Pdyn/KOR system (Crowley et al. 2016). Initial reports have identified the BNST as a mediator of stress responses to TMT in rats (Fendt et al. 2003). We tested whether microinfusions of norBNI directly into the BNST would also alter behavioral responses to TMT during protracted abstinence [Fig 1G, Fig 1 Suppl 2A]. Similar to systemic administration, intra-BNST norBNI reduced heightened contact with TMT in the EtOH mice [Fig 1H-J] with no effect on time spent in the far corners of the home cage [Fig 1K]. EtOH mice showed significantly less burying behavior in response to TMT compared to H_2O mice, but there was no effect of drug [Fig 1L].

We then tested if Pdyn neurons in the BNST played a role in this process, as we have previously shown that BNST Pdyn can modulate synaptic transmission in the BNST (Crowley et al. 2016). *Pdyn* was deleted from the BNST using the *Pdyn*$^{lox/lox}$ mouse line (Bloodgood et al. 2019) via AAV Cre-GFP microinfusions [Fig 1M-N, Fig 1 Suppl 2B]. EtOH mice with BNST Pdyn deletion did not show EtOH-impaired increases in TMT contact [Fig 1O-P], and floxed mice increased burying behavior compared to control EtOH mice [Fig 1R]. Importantly, there

were no effects of Pdyn deletion in H_2O drinkers. This rescue of TMT response in Pdyn deletion EtOH mice was not related to differences in EtOH consumption compared to GFP controls [Fig 1 Suppl 1H-K]. These findings demonstrate a role for BNST Pdyn/KOR in regulating specific behavioral responses impaired by long-term EtOH drinking.

Previous studies in rats have shown that TMT increases BNST activity using c-Fos as a marker for active neuronal populations (Day et al. 2004, Asok et al. 2013), so we examined this in a line of *Pdyn*-IRES-Cre x Rosa26-flox-stop-L10-GFP (Pdyn-GFP) mice (Al-Hasani et al. 2015) after intermittent EtOH or H_2O consumption [Fig 2A]. TMT elicited robust dorsal BNST c-Fos immunostaining, which was greater in EtOH mice compared to H_2O mice [Fig 2B-C]. Furthermore, TMT increased expression of Pdyn GFP-expressing neurons in the BNST versus non-stressed (NS) mice [Fig 2D]. Importantly, colocalization of c-Fos in Pdyn-containing cells (BNST^{PDYN}) was largest in the stressed EtOH group [Fig 2E], suggesting an interaction between EtOH and predator odor stress in the BNST.

To assess dynamic BNST^{PDYN} responses to TMT in real-time, we performed *in-vivo* fiber photometry in EtOH and H_2O mice. Pdyn-Cre mice were injected with a viral construct containing a Cre-inducible genetically-encoded calcium indicator (FLEX-GCaMP7f) and optical fibers were implanted above the BNST [Fig 2F-G, Fig 2 Suppl 2]. When averaged across three TMT exposures, both H_2O and EtOH mice showed sustained increases in BNST^{PDYN} calcium activity in response to TMT [Fig 2H], which were larger than calcium transients in response to double distilled water (DDW). However, while BNST^{PDYN} responses in H_2O mice did not habituate across trials, EtOH mice displayed reduced BNST^{PDYN} responses in the third TMT trial compared to the first TMT trial [Fig 2I], suggestive of a blunted stress response. These results

indicate that rapid suppression of BNST^{PDYN} activity to stress cues may drive aberrant behavioral responses after chronic drinking.

We next examined the synaptic activity of BNST^{PDYN} neurons following TMT exposure by recording spontaneous excitatory and inhibitory post-synaptic currents (sEPSC, sIPSC) in Pdyn-GFP mice during 7-10 days protracted abstinence [Fig 3A]. TMT increased sEPSC frequency (Hz) in EtOH and H_2O drinkers compared to non-stressed (NS) mice [Fig 3B] with no alterations in sIPSC frequency [Fig. 3C]. EtOH and TMT did not impact sEPSC and sIPSC amplitude [Fig 3 Suppl 1A-B]. Increased sEPSC/sIPSC ratios also reflected heightened excitatory drive onto BNST^{PDYN} cells in stressed mice regardless of drinking history [Fig 3D]. We were curious if this was an emergent property, similar to incubation of craving, or if this was engaged early in abstinence. To test this, we performed similar experiments and found that during early abstinence, activity of BNST^{PDYN} neurons is suppressed following alcohol drinking, yet robustly and synergistically engaged following repeated swim exposure in EtOH drinking mice [Fig 3 Suppl 1C-E]. We next sought to examine if KOR played a role in driving this cellular phenotype. Systemic norBNI pretreatment reduced sEPSC frequency in BNST^{PDYN} cells [Fig 3E-F], but not sIPSC frequency [Fig 3G], with an increase in the sEPSC/sIPSC ratio being suppressed by norBNI in the EtOH TMT mice [Fig 3H]. NorBNI did not alter sEPSC or sIPSC amplitude in stressed mice [Fig 3 Suppl 1F-G]. Recordings from non-GFP cells after EtOH and stress [Fig 3 Suppl 1H-K] also revealed heightened sEPSC/sIPSC ratios [Fig 3 Suppl 1J], indicating a general increase in glutamatergic transmission in the BNST. These *ex-vivo* experiments demonstrate that exposure to stress and EtOH induces KOR-mediated alteration of synaptic transmission in the BNST.

To characterize EtOH and stress-specific enhancement of glutamate transmission to the BNST, we labeled inputs to the BNST with the retrograde fluorophore choleratoxin B (CTB) [Fig 4 Suppl 1A] and assessed colocalization with c-Fos following exposure to TMT in EtOH and H_2O mice. Among the known glutamatergic BNST projections, the medial prefrontal cortex (mPFC) showed the largest number of activated inputs, marked by c-Fos and CTB colocalization, in stressed EtOH mice [Fig 4 Suppl 1C; other known projection regions: insula (Fig 4 Suppl 1D) and amygdala (Fig 4 Suppl 1E)]. Since we have previously reported increased glutamatergic transmission in the mPFC following acute TMT exposure (Hwa et al. 2019), we wanted to investigate if EtOH and TMT together may strengthen the functional connection between mPFC-BNST.

To investigate the role of mPFC projections to the BNST in alcohol-induced responses to stress, we injected an AAV encoding channelrhodopsin (ChR2) into the mPFC of Pdyn-GFP mice [Fig 4A] and measured BNST cell responses to photostimulation of this pathway using slice electrophysiology [Fig 4 Suppl 1I-K]. A greater proportion of BNST^{PDYN} neurons were light-responsive after TMT in both H_2O and EtOH mice, whereas non-stressed H_2O mice had mostly non-responsive cells [Fig 4B]. Similarly, EtOH mice had larger monosynaptic optically-evoked EPSC (oEPSC) amplitudes following TMT compared to H_2O mice and non-stressed EtOH mice [Fig 4C], with no effects on paired pulse ratio [Fig 4D]. Both AMPA and NMDA peak amplitudes were greater in BNST^{PDYN} EtOH TMT mice compared to unstressed EtOH mice and H_2O mice [Fig 4E-F]. There was also an increase in the AMPA/NMDA ratio in the EtOH TMT mice [Fig 4G], suggesting alcohol drinking may prime the synapse for AMPA receptor recruitment, further contributing to aberrant glutamate signaling and stress reactions. In addition,

the EtOH TMT mice were also more resistant to synaptic depression using oEPSC pulse train protocols, suggesting alterations in short-term plasticity [Fig 4H-K].

Discussion

Here, we have characterized alcohol-induced deficits in stress reactions to TMT predator odor. First, we identified BNST^{PDYN} as a stress- and alcohol-sensitive population using immunohistochemistry and fiber photometry. With whole cell patch clamp electrophysiology, we found that enhanced synaptic drive in BNST^{PDYN} cells was reduced by KOR antagonism in stressed mice with a history of alcohol drinking. Finally, experiments with *ex vivo* optogenetics indicated that EtOH-drinking stressed mice had increased prefrontal cortical synaptic connectivity onto BNST^{PDYN} cells compared to stressed H_2O drinkers and unstressed EtOH drinkers. Altogether, our findings indicate that engagement of Pdyn/KOR signaling in the BNST promotes an allostatic shift in stress-coping following EtOH drinking.

BNST KOR/Pdyn gates stress reactions after EtOH

These findings support a role for Pdyn/KORs in the extended amygdala in altering stress coping phenotypes in heavy drinkers. Weeks of intermittent access to EtOH affected KOR-sensitive stress reactions in multiple modalities, including the repeated swim test and exposure to TMT predator odor. Using converging approaches of intra-BNST norBNI infusions and a genetic deletion of BNST^{PDYN} using a floxed mouse line, we show that reducing Pdyn/KOR signaling at the pre- or post-synaptic level, respectively, normalizes alcohol-induced impairments in stress reactions to TMT during protracted abstinence. These results are in line with literature showing KOR antagonists can block anxiety-like behaviors precipitated by acute withdrawal from alcohol vapor (Valdez and Harshberger 2012, Rose et al. 2016) and suppress alcohol self-administration

in post-dependent rats (Walker and Koob 2008, Schank et al. 2012, Kissler et al. 2014). KORs in the BNST appear to be particularly important in mediating interactions between stress and alcohol drinking, as BNST norBNI attenuates stress-induced alcohol seeking (Lê et al. 2018) and reduces alcohol withdrawal-induced 22-kHz ultrasonic vocalizations (Erikson et al. 2018). While this previous research has established that there is critical involvement of this stress peptide system in promoting acute alcohol withdrawal behaviors, we demonstrate here that KOR is still engaged in protracted abstinence, particularly during episodes of high stress exposure. Taken together, this body of evidence suggests that KOR signaling in the BNST is a critical pharmacological target for treatment of alcohol use disorders.

Our findings using c-Fos immunolabeling show that BNST^{PDYN} cells are synergistically engaged in responses to stressors in EtOH-drinking mice. This complements existing c-Fos work in the BNST after TMT predator odor (Day et al. 2004, Asok et al. 2013, Janitzky et al. 2015) while newly connecting the Pdyn population with changes in stress responses following a history of EtOH drinking. While c-Fos expression is indicative of active populations with low temporal resolution, we further observed real-time engagement of BNST^{PDYN} cells during the TMT exposure using cell-specific fiber photometry. BNST^{PDYN} calcium transients robustly increased after the initial TMT exposure in both H_2O and EtOH mice, consistent with specific subpopulations of BNST neurons that exhibit TMT-elicited calcium transients (Giardino et al. 2018). However, upon repeated exposures to TMT, EtOH mice exhibited a decrease in calcium activity, suggesting a potential circuit substrate of habituation to the stressor. We interpret this decrease in percent change from first TMT exposure as a loss of salience of the predator odor over time, which may explain the EtOH-induced increase in TMT contact during behavioral tests.

Glutamatergic contribution to stress-enhanced signaling in BNST^{PDYN} neurons

After assessing population activity of BNST PDYN/KOR after EtOH and stress and the contributions of this population to drinking-induced alterations in behavior, we performed synaptic transmission experiments on BNST^{PDYN} neurons during acute and protracted abstinence from EtOH. Repeated forced swim stress increased synaptic drive in EtOH drinkers, suggesting a metaplastic shift and increased sensitivity of the circuit during early 24 hr withdrawal. In addition, there were trends towards non-stressed intermittent EtOH mice having increased sIPSC frequency in BNST^{PDYN} cells. Others have reported increased sIPSC frequency in the BNST 24 hr after drinking in monkeys, but also increased sEPSC/sIPSC ratio in C57BL/6J mice 48 hr after ethanol vapor (Pleil et al. 2015; Pleil et al. 2016), so our cell-specific recordings, different drinking/exposure protocols, and withdrawal time points may be reasons for differences. During protracted abstinence, there were no apparent synaptic transmission differences between withdrawn mice and controls, although previous reports have found increased sEPSC frequency at this time point in female drinkers in a BNST CRF population (Centanni et al. 2019). Rather, we found that TMT increased glutamatergic transmission in both BNST^{PDYN+} and BNST^{PDYN-} neurons after EtOH and TMT, suggesting enhanced glutamatergic activity across the region. While BNST^{PDYN} synaptic drive did not differ between stressed H_2O and EtOH mice, differences were revealed during KOR blockade with norBNI pretreatment. Altogether, while other studies have found that chronic EtOH exposure and withdrawal can impact BNST spontaneous glutamatergic and NMDAR function (Kash et al. 2009, Wills et al. 2012, McElligott and Winder 2009), our findings are the first to highlight plastic shifts in response to stressors as well as identifying pathway-specific alterations in neuropeptide signaling.

EtOH and stress interact revealing synaptic plasticity from cortical input

Using retrograde fluorescent labeling, we identified the mPFC, among other brain regions, as a glutamatergic source of increased excitatory signaling onto BNST^{PDYN} neurons after stress and EtOH. Previous work in the lab found that both the central amygdala (CeA) and basolateral amygdala (BLA) inputs to the BNST are KOR-sensitive, but mPFC inputs are KOR-insensitive (Crowley et al. 2016). Notable, photostimulation of BLA inputs promotes anxiolysis (Crowley et al. 2016). Taken together, this suggests a model in which increased activity of BNST^{PDYN} neurons can promote release of Pdyn, which would inhibit amygdala inputs to the BNST and promote increased engagement of mPFC glutamate signaling. We have previously identified PL layer 2/3 neurons as a population engaged in response to acute TMT using a combination of slice physiology and immunohistochemical approaches (Hwa et al. 2019), providing converging data for engagement of this pathway by this specific aversive stimulus. This finding stands in contrast to Pdyn/KOR signaling in the CeA, which appears to promote alcohol consumption (Bloodgood et al. 2019).

Our experiments further explore the synaptic strength of mPFC to BNST pathway through activating BNST^{PDYN} cells by optical stimulation of CamKIIa-labeled mPFC inputs. A higher proportion of BNST^{PDYN} neurons were light-responsive following stress or EtOH compared to H_2O controls, suggesting that these stimuli increase connectivity between the mPFC and BNST^{DYN} neurons. Taking into account the observed increased oEPSC, AMPA, and NMDA amplitudes and AMPA/NMDA ratio after the combination of EtOH and TMT, it seems that EtOH exposure primes the synapse for aberrant responses to stressors under the control of a glutamatergic mechanism. Further, with repeated stimulation pulse trains, the EtOH TMT BNST^{PDYN} cells show reduced short-term depression, suggesting increased fidelity and short-term plasticity. Again, this is in line with known chronic EtOH-induced glutamate plasticity in

BNST cells (Wills et al. 2012). Future experiments should compare the mPFC projection with other known glutamatergic inputs such as the BLA in these *ex vivo* optogenetic protocols to confirm the pathways underlying stress-EtOH interactions.

BNST circuitry control of stress behavior

A recent paper from the Radley lab explored the prelimbic (PL) region of the mPFC to BNST pathway in stress-related behaviors in rats using optogenetics (Johnson et al. 2019). Activation of the PL to BNST circuit negatively correlated with freezing behavior, a measure of passive coping, in response to a shock prod, while photoinhibition increased freezing and decreased burying, a measure of active coping. Notably, they found that these behavioral effects were related to downstream control of the periaqueductal gray. An important future direction will be to assess the role of specific downstream projection targets of BNST dynorphin neurons, including the periaqueductal gray. It is also possible that excitatory local microcircuity in the BNST activates GABA neurons that inhibit ventral tegmental area GABA output signaling reward, which leads to anhedonia-like behavior and reduced stress coping. These findings on aberrant stress coping during protracted withdrawal from alcohol complement established research characterizing the extended amygdala to BNST anxiolytic-like circuitry using chemo- and optogenetics in mice (Kim et al. 2013, Jennings et al. 2013, Marcinkiewcz et al. 2016, Mazzone et al. 2018, Crowley et al. 2016).

Conclusions

Maladaptive responses to stress are a hallmark of alcohol use disorder, but the mechanisms that underlie this are not well characterized. Here we show that KOR signaling in the BNST is a critical molecular substrate disrupting stress-coping behavior following heavy alcohol drinking. These findings suggest that increased corticolimbic connectivity may underlie

impaired stress-coping during protracted withdrawal from heavy drinking and represents a potential biomarker of negative outcomes. Disentangling this imbalance of stress neuropeptide signaling may lead to the development of therapeutics to enhance stress coping in persons with alcohol use disorder.

Materials and Methods

Animals. Eight-week old male C57BL/6J mice (Jackson Laboratories, Bar Harbor, ME) were used for behavioral pharmacology experiments. To visualize Pdyn-expressing neurons, we generated a Pdyn-GFP reporter line by crossing *preprodynorphin*-IRES-Cre mice (Crowley et al. 2016, Bloodgood et al. 2019, Al-Hasani et al. 2015) (Pdyn-Cre) and Rosa26-flox-stop-L10-GFP reporter mice. For conditional knockout of BNST Pdyn, we used the *Pdyn$^{lox/lox}$* mouse line (Bloodgood et al. 2019). These mice were bred in the UNC facilities. All mice were group-housed for at least 3 days before being singly housed in polycarbonate cages (GM500, Tecniplast, Italy) with a 12:12-h reversed dark-light cycle with lights off at 7:00am. Mice had unrestricted access to food (Prolab Isopro RMH 3000, LabDiet, St. Louis, MO) and H_2O. The UNC School of Medicine Institutional Animal Care and Use Committee approved all experiments. Procedures were conducted in accordance with the NIH Guidelines for the Care and Use of Laboratory Animals.

Intermittent EtOH Drinking. Mice were given 24 hr access to a 20% (w/v) EtOH solution and water on an intermittent schedule (Hwa et al. 2011). Two bottles were held in modified drinking spouts of plastic cage tops and weighed before and after daily EtOH access. A dummy cage without an animal was used to simulate fluid lost while positioning the bottles, so average fluid drip was subtracted from each mouse's daily drinking. Mice were tested for stress reactions to TMT during 7-10 day protracted abstinence after 6 weeks of intermittent drinking. Separate

groups of mice were tested for stress reactions to forced swim and TMT predator odor after 8 weeks of intermittent drinking.

Behavioral Assays after EtOH Drinking

Repeated Forced Swim Test. Mice were placed into an acrylic cylinder filled with 23-25° water 4 hr before access to EtOH for 10 min (Anderson et al. 2016). Immobility duration was hand-scored by a blind observer across two trials. Increases in immobility time across forced swim trials were interpreted as an adaptive stress coping strategy (Commons et al. 2017).

TMT Predator Odor Exposure. Exposure to fox-derived synthetic predator odor, trimethylthiazoline (TMT), was performed in the home cage as previously described to elicit stress reactions in mice (Hwa et al. 2019). For a baseline pre-trial period, mice habituated to a cotton tip applicator held vertically in place for 10 min in the home cage. The TMT trial occurred when 2.5 µl TMT was applied to the cotton tip followed by 10 min of behavioral observation. Duration of contact with the TMT object, time spent in the far corners of the cage, and distance traveled (sec) were recorded and quantified with Ethovision XT13 (Noldus, The Netherlands), and burying was hand-scored using BORIS (Behavioral Observation Research Interactive Software) by a blind observer. Heatmaps were generated through Ethovision XT13.

Stereotaxic Surgery. Adult mice (>8 weeks) were deeply anesthetized with 3-4% isoflurane in oxygen and placed into a stereotaxic frame (Kopf Instruments, Tujunga, CA) while on a heated pad. Isoflurane anesthesia was maintained at 1-2% during the remainder of the surgery. After sterilization with 70% ethanol and betadine, a scalp incision was made and burr holes were drilled above the target. A 1 µl Neuros Hamilton syringe (Hamilton, Reno, NV) microinjected the virus or drug at a rate of 0.1 µl/min. Coordinates for the BNST were AP +0.30 mm, ML +/- 0.95 mm, DV -4.35 mm from bregma. Coordinates for the mPFC were AP +1.70 mm, ML +/-

0.30 mm, DV -2.50 mm from bregma. For fiber photometry surgery, both virus and 4.5 mm ceramic ferrules (Neurophotometrics Ltd, CA) were implanted at a 10° angle. Mice recovered for one week before testing.

Drugs and Viral Vectors. 5 mg/kg norBNI (Cat no. 0347, Tocris) was administered i.p., 1ml/100g, 16 hr before testing to both EtOH and H_2O mice. For intra-BNST norBNI microinfusions, 5 ug/ul norBNI was injected with 50 nl AAV5-CamKII-eGFP to mark the injection site. *Pdyn*$^{lox/lox}$ mice received 300 nl AAV5-CamKII-Cre-eGFP (UNC Vector Core, Lot 6450) and control AAV5-CamKII-eGFP (Lot 4621B) in the BNST. Fiber photometry experiments used 300 nl AAV9-syn-FLEX-GCaMP7f and ceramic ferrules in Pdyn-Cre mice. Choleratoxin B (CTB) 555 (Invitrogen) was used for retrograde tracing injected 7 days before testing. 300 nl AAV5-CamKIIa-hChR2(H134R)-mCherry-WPRE-hGH (Addgene, Lot CS1096) was injected into the mPFC of Pdyn-GFP mice for synaptic connectivity experiments in the BNST. All intracranial injections were bilateral.

c-Fos Immunohistochemistry, Histology, and Microscopy. Mice were deeply anesthetized with Avertin before transcardial perfusion with phosphate buffered saline and 4% paraformaldehyde. Brains were extracted, cryoprotected, and then sliced on a Leica 1200S vibratome. Coronal sections of the Pdyn-GFP mice were stained for *c-Fos* immunofluorescence to visualize colocalization of Pdyn-containing (GFP) and *c-Fos* expressing cells. In separate mice, the retrograde fluorescent tracer choleratoxin B (CTB) 555 was injected into the BNST of C57BL/6J mice. The immunofluorescence protocol for *c-Fos* was performed according to previous studies (Hwa et al. 2019) using tyramine signal amplification (TSA). After PBS washes, 50% methanol, and 3% hydrogen peroxide, tissue was incubated in blocking buffer with 0.3% Triton X-100 and 1% bovine serum albumin for 60 min. Slices were then incubated at 4°C for 48 hr in blocking

buffer containing a rabbit anti-*c-Fos* antibody (1:3000, ABE457, Millipore, Bellerica, MA). After washes in TNT (0.1 M Tris-HCl, 0.15 M NaCl, 3% TritonX-100) and TNB (0.1 M Tris-HCl, 0.15 M NaCl, 0.5% Perkin Elmer blocking reagent) buffer, slices were incubated in a goat anti-rabbit horse radish peroxidase-conjugated IgG (1:200, NEF812001EA, PerkinElmer, Waltham, MA) for 30 min. After TNT washes, tissue was processed using a TSA kit with Cy3-tyramide (1:50, PerkinElmer, Waltham, MA) for 10 min. For placement verification, viral injection sites were verified using a wide-field epifluorescent microscope (BX-43, Olympus, Waltham, MA). For quantification of *c-Fos* immunofluorescence and CTB tracing, slices were imaged on a Zeiss 800 laser scanning confocal microscope (Carl Zeiss, Germany) and analyzed with Zeiss Zen 2 Blue Edition software.

Fiber photometry

Apparatus. A branched fiber optic patch cord (Doric Lenses, BFP_200/230/900-0.37_FC-MF1.25) connected to the fiber photometry apparatus (Neurophotometrics, Ltd.) was attached bilaterally to implanted fiber optic cannulae using cubic zirconia sleeves. To record fluorescence signals from GCaMP7f, light from a 470 nm LED was bandpass filtered, collimated, reflected by dichroic mirrors, and focused by a 20x objective. LED light was delivered at a power that resulted in 35-50 µW of 470 nm light at the tip of the patch cord. Emitted GCaMP7f fluorescence was bandpass filtered and focused on the sensor of a CCD camera. The end of the fiber was imaged at a rate of 40 frames per sec, and the mean value of a ROI of a cross-section of the fiber was calculated using the open-source software Bonsai. To serve as an isosbestic control channel, 415 nm LED light was delivered sequentially with 470 nm LED light in a similar manner. Recording data were aligned with behavior using keystroke timestamps for behavioral video capture start.

Analysis. Analysis of fiber photometry signals was performed using custom-written MATLAB code (Mathworks, Inc.). GCaMP7f (470 nm) and isosbestic (415 nm) signals were de-interleaved, low-pass filtered (2 Hz), fit with a biexponential curve that was then subtracted from filtered data to correct for bleaching, and normalized by calculating the change from mean fluorescence (ΔF/F) and z-scoring. Odor-associated GCaMP7f activity was determined by calculating the AUC of transients aligned to the completion of odor delivery.

Behavior. To record from BNST^{PDYN} neurons in response to TMT, Pdyn-Cre mice were injected with AAV-FLEX-GCaMP7f and ferrules were implanted above the BNST. Mice were habituated to patch cords for three days before odor testing. On the day of odor testing, mice were exposed to three sequential trials each of double distilled water (DDW) and the predator odor TMT in the home cage. Two min of baseline recordings were collected before odor delivery and recording continued for 5 min following odor delivery. To minimize the role of the experimenter during testing, the odors were delivered via syringe pump attached to polyethylene tubing. The liquid odors were contained between air bubbles and DDW to prevent odor leak prior to intended delivery.

Slice Electrophysiology. Ninety minutes following TMT, which was also 24 hr after the last EtOH access, mice were sacrificed via deep isoflurane anesthesia, and coronal brain slices containing the BNST were collected according to standard laboratory protocols (Hwa et al. 2019, Crowley et al. 2016, Bloodgood et al. 2019). Whole-cell voltage-clamp electrophysiological recordings were performed in BNST^{PDYN} cells visualized using a 470 nm LED. The effects of EtOH and TMT on basal synaptic transmission were assessed in voltage clamp by adjusting the membrane potential and using a cesium methanesulfonate-based intracellular solution (135 mM cesium methanesulfonate, 10 mM KCl, 10mM HEPES, 1 mM MgCl2, 0.2 mM EGTA, 4 mM

MgATP, 0.3 mM GTP, 20 mM phosphocreatine, pH 7.3, 285-290 mOsmol). Lidocaine n-ethyl bromide (1 mg/ml) was included in the intracellular solution to block postsynaptic sodium currents. Neurons were held at -55 mV to assess glutamatergic synaptic transmission. In the same cell, neurons were held at +10 mV to assess GABAergic synaptic transmission. Fluctuations in current were used to determine spontaneous post-synaptic current (sEPSC or sIPSC) frequency and amplitude, as well as to calculate sEPSC/sIPSC ratios. Synaptic transmission experiments in BNST^{PDYN} cells were also performed in animals that received 5 mg/kg norBNI i.p. 16 hr prior to TMT. Electrophysiological recordings were then analyzed using Clampfit 10.7 software (Molecular Devices, Sunnyvale, CA).

For *ex-vivo* optogenetic experiments, tissue was evaluated for light-evoked action potentials in the mPFC. Brains were discarded and not used for further experimentation if injection sites were missed or if action potentials were not present. A blue LED (470 nm, CoolLed) was used to optically stimulate release from channelrhodopsin (ChR2)-containing fibers (Crowley et al. 2016). Picrotoxin (25 uM), tetrodotoxin (500 nM), and 4-AP (200 uM) were added to the aCSF to isolate monosynaptic oEPSCs with cells held at -70 mV. The intracellular solution was cesium gluconate (117 mM D-gluconic acid and cesium hydroxide, 20 mM HEPES, 0.4 mM EGTA, 5 mM tetraethyl ammonium chloride, 2 mM MgCl26H2O, 4 mM Na2ATP, 0.4 Na2GTP, pH 7.3, 287-292 mOsmol). oEPSC amplitude (pA) was the first peak of the paired pulse ratio with a 50 ms interstimulus interval. Paired pulse ratio was calculated as the second peak amplitude divided by the first peak amplitude. Cells were held at -70 mV to isolate AMPAR-mediated current and at +40 mV for NMDAR-mediated current. In separate slices, ten 1, 5, and 10 Hz pulse trains were performed at -55 mV voltage clamp without the presence of

ionotropic inhibitors with the cesium methanesulfonate internal solution. The nine subsequent amplitudes in the pulse train were normalized to the first peak.

Statistics. Time spent in contact with the TMT, far corners, and burying behavior in sec were analyzed with two-way ANOVA with drug/virus and EtOH as factors. Post-hoc paired and unpaired t-tests were two-tailed and used where appropriate as described in Figure Legends. In experiments where virus was injected before EtOH, cumulative 6-week alcohol intake and average ethanol preference were compared via t-test. BNST *c-Fos*, Pdyn-containing, and *c-Fos* and Pdyn colocalization were analyzed with two-way ANOVA with TMT exposure and EtOH as factors. Fiber photometry ΔF/F calcium signals were transformed into z-scores and area under the curve. Responses between TMT trial 1 and trial 3 were compared with a paired t-test. Synaptic transmission measures (e.g. sEPSC frequency) were analyzed with two-way ANOVA with TMT exposure and EtOH as factors. With norBNI physiology, only stressed mice with no injection were compared with norBNI-injected stressed mice in separate two-way ANOVA with drug and EtOH as factors. To compare proportion of light-responsive cells per condition, a X^2 test was performed. Furthermore, optically-evoked experiments (e.g. oEPSC amplitude) were analyzed with two-way ANOVAs comparing TMT and EtOH exposure. Pulse trains were analyzed with repeated measures two-way ANOVA across stimulus time and condition. Alpha was set to 0.05. Biological replicates throughout behavioral, immunohistochemical, and electrophysiological studies were combined. Statistical tests were analyzed with GraphPad Prism 8 (La Jolla, CA, USA).

Acknowledgments

Funding: This work was supported by the National Institutes of Health [grant numbers K99AA027576 (LSH), T32AA007573 (MEF), F32AA026485 (MMP), F31AA027129 (WY), R01AA019454 (TLK), U01AA020911 (TLK), and R01AA025582 (TLK)].

Author Contributions: LSH, SN, CS, EK, and RC performed and analyzed behavioral tests. LSH, MEF, and OH provided support for and analyzed the fiber photometry experiments. LSH, SN, MMP, and DP assisted with electrophysiology experiments. WY and KB provided additional technical expertise. LSH and TLK conceptualized, designed the study, and wrote the manuscript.

References

Anderson, R. I., Lopez, M. F., & Becker, H. C. (2016). Forced swim stress increases ethanol consumption in C57BL/6J mice with a history of chronic intermittent ethanol exposure. *Psychopharmacology*, *233*(11), 2035-2043.

Asok, A., Ayers, L. W., Awoyemi, B., Schulkin, J., & Rosen, J. B. (2013). Immediate early gene and neuropeptide expression following exposure to the predator odor 2, 5-dihydro-2, 4, 5-trimethylthiazoline (TMT). *Behavioural brain research*, *248*, 85-93.

Becker, H. C., Lopez, M. F., & Doremus-Fitzwater, T. L. (2011). Effects of stress on alcohol drinking: a review of animal studies. *Psychopharmacology*, *218*(1), 131.

Bloodgood, D. W., Pati, D., Pina, M. M., Neira, S., Hardaway, J. A., Desai, S., ... & Kash, T. L. (2019). Kappa Opioid Receptor and Dynorphin Signaling in the Central Amygdala Regulates Alcohol Intake. *bioRxiv*, 663666.

Bruchas, M. R., Land, B. B., Lemos, J. C., & Chavkin, C. (2009). CRF1-R activation of the dynorphin/kappa opioid system in the mouse basolateral amygdala mediates anxiety-like behavior. *PloS one*, *4*(12), e8528.

Centanni, S. W., Morris, B. D., Luchsinger, J. R., Bedse, G., Fetterly, T. L., Patel, S., & Winder, D. G. (2019). Endocannabinoid control of the insular-bed nucleus of the stria terminalis circuit regulates negative affective behavior associated with alcohol abstinence. *Neuropsychopharmacology*, *44*(3), 526.

Commons, K. G., Cholanians, A. B., Babb, J. A., & Ehlinger, D. G. (2017). The rodent forced swim test measures stress-coping strategy, not depression-like behavior. *ACS chemical neuroscience*, *8*(5), 955-960.

Crowley, N. A., Bloodgood, D. W., Hardaway, J. A., Kendra, A. M., McCall, J. G., Al-Hasani, R., ... & Lowell, B. B. (2016). Dynorphin controls the gain of an amygdalar anxiety circuit. *Cell reports*, *14*(12), 2774-2783.

Day, H. E., Masini, C. V., & Campeau, S. (2004). The pattern of brain c-fos mRNA induced by a component of fox odor, 2, 5-dihydro-2, 4, 5-trimethylthiazoline (TMT), in rats, suggests both systemic and processive stress characteristics. *Brain research*, *1025*(1-2), 139-151.

Erikson, C. M., Wei, G., & Walker, B. M. (2018). Maladaptive behavioral regulation in alcohol dependence: Role of kappa-opioid receptors in the bed nucleus of the stria terminalis. *Neuropharmacology*, *140*, 162-173.

Fendt, M., Endres, T., & Apfelbach, R. (2003). Temporary inactivation of the bed nucleus of the stria terminalis but not of the amygdala blocks freezing induced by trimethylthiazoline, a component of fox feces. *Journal of Neuroscience*, *23*(1), 23-28.

Giardino, W. J., Eban-Rothschild, A., Christoffel, D. J., Li, S. B., Malenka, R. C., & de Lecea, L. (2018). Parallel circuits from the bed nuclei of stria terminalis to the lateral hypothalamus drive opposing emotional states. *Nature neuroscience*, *21*(8), 1084.

Gilpin, N. W., & Weiner, J. L. (2017). Neurobiology of comorbid post-traumatic stress disorder and alcohol-use disorder. *Genes, Brain and Behavior*, *16*(1), 15-43.

Heilig, M., Egli, M., Crabbe, J. C., & Becker, H. C. (2010). Acute withdrawal, protracted abstinence and negative affect in alcoholism: are they linked? *Addiction biology*, *15*(2), 169-184.

Hwa, L. S., Chu, A., Levinson, S. A., Kayyali, T. M., DeBold, J. F., & Miczek, K. A. (2011). Persistent escalation of alcohol drinking in C57BL/6J mice with intermittent access to 20% ethanol. *Alcoholism: Clinical and Experimental Research*, *35*(11), 1938-1947.

Hwa, L. S., Neira, S., Pina, M. M., Pati, D., Calloway, R., & Kash, T. L. (2019). Predator odor increases avoidance and glutamatergic synaptic transmission in the prelimbic cortex via corticotropin-releasing factor receptor 1 signaling. *Neuropsychopharmacology*, *44*(4), 766.

Janitzky, K., Kröber, A., & Schwegler, H. (2015). TMT predator odor activated neural circuit in C57BL/6J mice indicates TMT-stress as a suitable model for uncontrollable intense stress. *Brain research*, *1599*, 1-8.

Jennings, J. H., Sparta, D. R., Stamatakis, A. M., Ung, R. L., Pleil, K. E., Kash, T. L., & Stuber, G. D. (2013). Distinct extended amygdala circuits for divergent motivational states. *Nature*, *496*(7444), 224.

Johnson, S. B., Emmons, E. B., Lingg, R. T., Anderson, R. M., Romig-Martin, S. A., LaLumiere, R. T., ... & Radley, J. J. (2019). Prefrontal–bed nucleus circuit modulation of a passive coping response set. *Journal of Neuroscience*, *39*(8), 1405-1419.

Kash, T. L. (2012). The role of biogenic amine signaling in the bed nucleus of the stria terminals in alcohol abuse. *Alcohol*, *46*(4), 303-308.

Kash, T. L., Baucum II, A. J., Conrad, K. L., Colbran, R. J., & Winder, D. G. (2009). Alcohol exposure alters NMDAR function in the bed nucleus of the stria terminalis. *Neuropsychopharmacology*, *34*(11), 2420.

Kim, S. Y., Adhikari, A., Lee, S. Y., Marshel, J. H., Kim, C. K., Mallory, C. S., ... & Malenka, R. C. (2013). Diverging neural pathways assemble a behavioural state from separable features in anxiety. *Nature*, *496*(7444), 219.

Kissler, J. L., Sirohi, S., Reis, D. J., Jansen, H. T., Quock, R. M., Smith, D. G., & Walker, B. M. (2014). The one-two punch of alcoholism: role of central amygdala dynorphins/kappa-opioid receptors. *Biological psychiatry*, *75*(10), 774-782.

Koob, G. F. (2009). Brain stress systems in the amygdala and addiction. *Brain research*, *1293*, 61-75.

Koob, G., & Kreek, M. J. (2007). Stress, dysregulation of drug reward pathways, and the transition to drug dependence. *American Journal of Psychiatry*, *164*(8), 1149-1159.

Le Merrer, J., Becker, J. A., Befort, K., & Kieffer, B. L. (2009). Reward processing by the opioid system in the brain. *Physiological reviews*, *89*(4), 1379-1412.

Lê, A. D., Funk, D., Coen, K., Tamadon, S., & Shaham, Y. (2018). Role of κ-opioid receptors in the bed nucleus of stria terminalis in reinstatement of alcohol seeking. *Neuropsychopharmacology*, *43*(4), 838.

Lutz, P. E., & Kieffer, B. L. (2013). Opioid receptors: distinct roles in mood disorders. *Trends in neurosciences*, *36*(3), 195-206.

Marcinkiewcz, C. A., Mazzone, C. M., D'Agostino, G., Halladay, L. R., Hardaway, J. A., DiBerto, J. F., ... & Tipton, G. J. (2016). Serotonin engages an anxiety and fear-promoting circuit in the extended amygdala. *Nature*, *537*(7618), 97.

Mazzone, C. M., Pati, D., Michaelides, M., DiBerto, J., Fox, J. H., Tipton, G., ... & Magness, S. T. (2018). Acute engagement of G q-mediated signaling in the bed nucleus of the stria terminalis induces anxiety-like behavior. *Molecular psychiatry*, *23*(1), 143.

McElligott, Z. A., & Winder, D. G. (2009). Modulation of glutamatergic synaptic transmission in the bed nucleus of the stria terminalis. *Progress in Neuro-Psychopharmacology and Biological Psychiatry*, *33*(8), 1329-1335.

Noone, M., Dua, J., & Markham, R. (1999). Stress, cognitive factors, and coping resources as predictors of relapse in alcoholics. *Addictive Behaviors*, *24*(5), 687-693.

Pleil, K. E., Helms, C. M., Sobus, J. R., Daunais, J. B., Grant, K. A., & Kash, T. L. (2016). Effects of chronic alcohol consumption on neuronal function in the non-human primate BNST. *Addiction biology*, *21*(6), 1151-1167.

Pleil, K. E., Lowery-Gionta, E. G., Crowley, N. A., Li, C., Marcinkiewcz, C. A., Rose, J. H., ... & Kash, T. L. (2015). Effects of chronic ethanol exposure on neuronal function in the prefrontal cortex and extended amygdala. *Neuropharmacology*, *99*, 735-749.

Rose, J. H., Karkhanis, A. N., Chen, R., Gioia, D., Lopez, M. F., Becker, H. C., ... & Jones, S. R. (2016). Supersensitive kappa opioid receptors promotes ethanol withdrawal-related behaviors and reduce dopamine signaling in the nucleus accumbens. *International Journal of Neuropsychopharmacology*, *19*(5).

Schank, J. R., Goldstein, A. L., Rowe, K. E., King, C. E., Marusich, J. A., Wiley, J. L., ... & Heilig, M. (2012). The kappa opioid receptor antagonist JDTic attenuates alcohol seeking and withdrawal anxiety. *Addiction biology*, *17*(3), 634-647.

Sinha, R., Fox, H. C., Hong, K. I. A., Hansen, J., Tuit, K., & Kreek, M. J. (2011). Effects of adrenal sensitivity, stress-and cue-induced craving, and anxiety on subsequent alcohol relapse and treatment outcomes. *Archives of general psychiatry*, *68*(9), 942-952.

Valdez, G. R., & Harshberger, E. (2012). Kappa opioid regulation of anxiety-like behavior during acute ethanol withdrawal. *Pharmacology Biochemistry and Behavior*, *102*(1), 44-47.

Walker, B. M., & Koob, G. F. (2008). Pharmacological evidence for a motivational role of κ-opioid systems in ethanol dependence. *Neuropsychopharmacology*, *33*(3), 643.

Wills, T. A., Klug, J. R., Silberman, Y., Baucum, A. J., Weitlauf, C., Colbran, R. J., ... & Winder, D. G. (2012). GluN2B subunit deletion reveals key role in acute and chronic ethanol sensitivity of glutamate synapses in bed nucleus of the stria terminalis. *Proceedings of the National Academy of Sciences*, *109*(5), E278-E287.

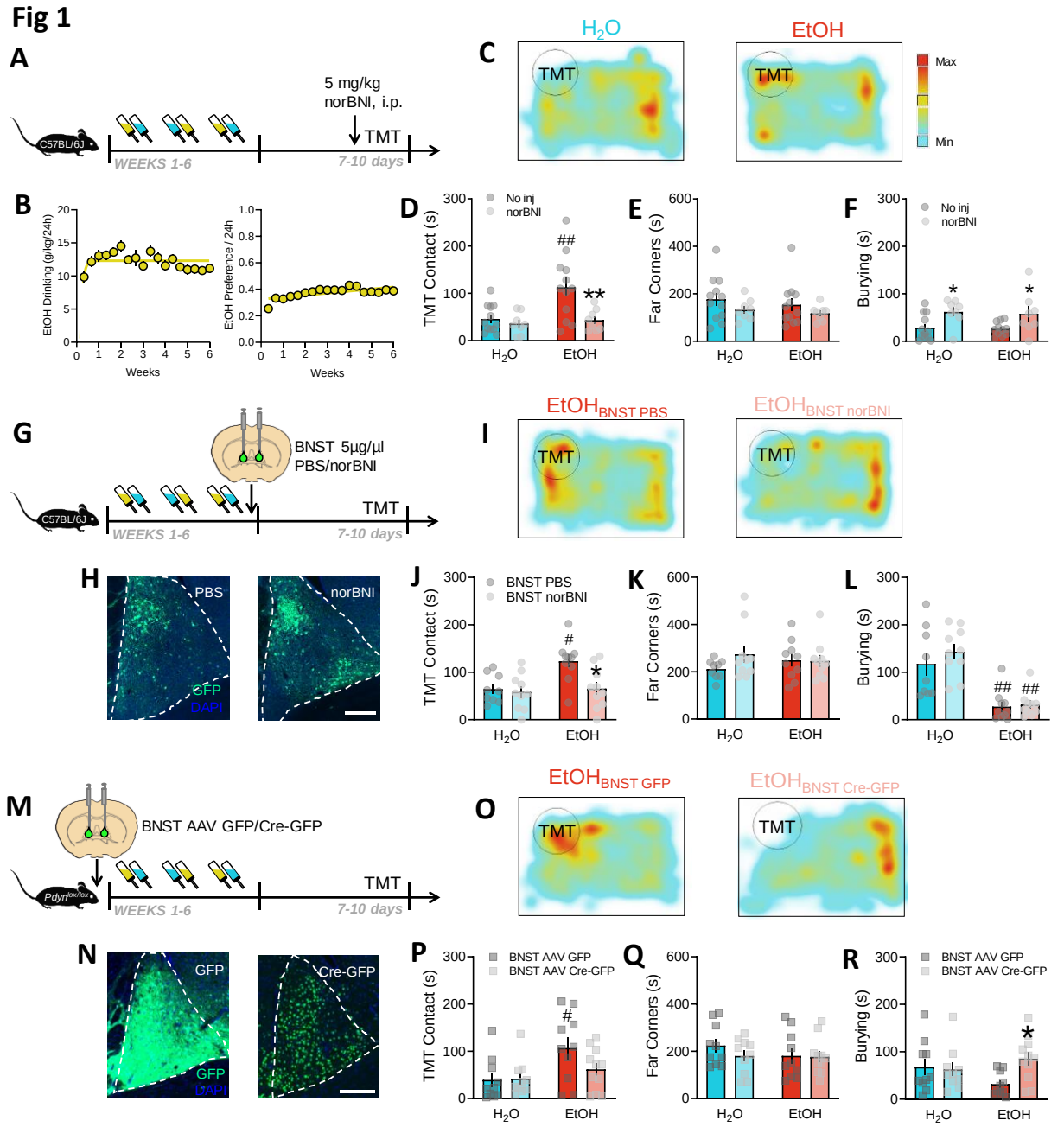

Fig 1. BNST KOR regulation of responses to TMT predator odor after long-term alcohol drinking. **A**, Experimental protocol for 5 mg/kg i.p. KOR antagonist manipulation of predator odor behavior after intermittent EtOH. **B**, EtOH drinking (g/kg/24hr) and preference / 24hr of male C57BL/6J mice included in a-f and g-l (n=24 mice). **C**, Representative heatmaps of individual H_2O (left) and EtOH (right) spatial location. The circle indicates TMT location. Red color indicates maximum time spent. Aqua color indicates minimum time spent. Pretreatment with norBNI affected: **D**, TMT contact (sec): interaction $F_{1,36}$=4.47, p=0.042; no injection H_2O vs EtOH t_{36}=3.75, ##p=0.0027; EtOH no injection vs norBNI t_{36}=3.48, **p=0.0012. **E**, Time spent in the far corners (sec), and **F**, Burying (sec): norBNI main effect $F_{1,36}$=12.08, p=0.0014; H_2O no injection vs norBNI t_{35}=2.56,

*p=0.0299; EtOH no injection vs norBNI t_{35}=2.36, *p=0.0472. **G**, Experimental design for 5 µg/µl norBNI in the BNST. **H**, Representative images of BNST infusions of PBS (n=9 H_2O, n=10 EtOH) and norBNI (n=10 H_2O, n=10 EtOH) marked with GFP. Scale bar indicates 200 µM. **I**, Representative heatmaps of TMT-induced activity with EtOH BNST PBS (left) and EtOH BNST norBNI (right). **J**, TMT contact (sec): interaction $F_{1,35}$=4.30, p=0.0454; PBS H_2O vs EtOH t_{35}=3.29, #p=0.0105; EtOH PBS vs norBNI t_{35}=3.32, *p=0.0105. **K**, Far Corners (sec). **L**, Burying (sec): EtOH main effect $F_{1,35}$=42.65, p<0.001; PBS H_2O vs EtOH t_{35}=4.06, ##p=0.0010; norBNI H_2O vs EtOH t_{35}=5.19, ##p<0.001. **M**, Time course of deletion of BNST Pdyn in *Pdyn$^{lox/lox}$* mice before EtOH and TMT. **N**, Images of AAV-GFP and AAV-Cre-GFP expression (H_2O GFP n=10, Cre-GFP n=10. EtOH GFP n=10, EtOH Cre-GFP n=11). Scale bar measures 200 µM. **O**, Sample TMT heatmaps of EtOH BNST GFP (left) and EtOH BNST Cre-GFP (right) mice. **P**, TMT contact (sec): EtOH main effect $F_{1,37}$=7.31, p=0.0103. GFP H_2O vs EtOH t_{37}=2.93, #p=0.0347. **Q**, Far Corners (sec). **R**, Burying (sec): interaction $F_{1,37}$=4.51, p=0.0405. EtOH GFP vs EtOH Cre-GFP t_{37}=3.91, *p=0.0419.

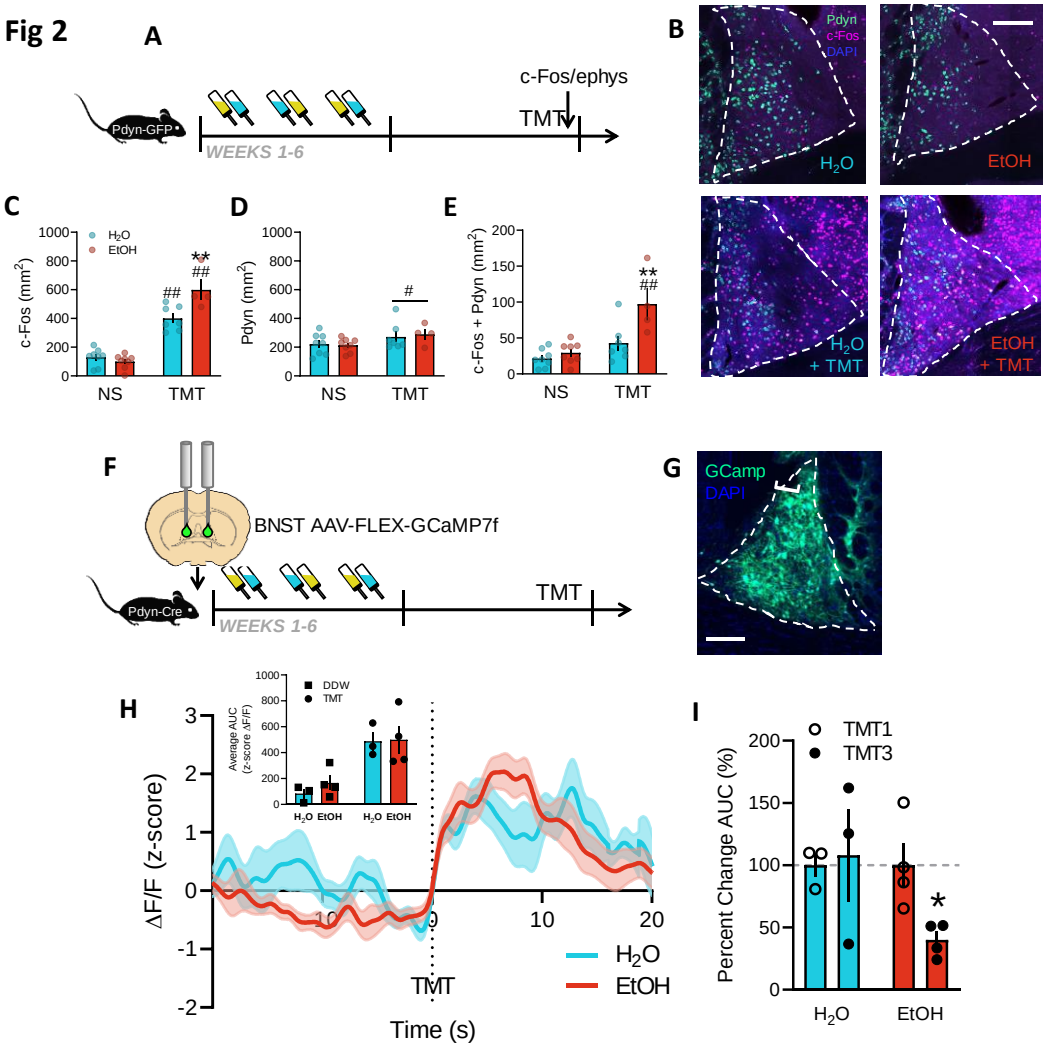

Fig 2. BNST as a critical site for prodynorphin neurons activated after stress during protracted withdrawal from alcohol. **A**, Schematic of obtaining BNST tissue for c-Fos immunohistochemistry or recording electrophysiology after EtOH and TMT in Pdyn-GFP mice. **B**, Representative images of Pdyn (green) and c-Fos Cy3 immunostaining (pseudocolored purple) in H_2O (n=8), EtOH (n=8), H_2O + TMT (n=7), and EtOH + TMT (n=4) conditions. Scale bar is 200 µm. **C**, BNST c-Fos quantification (mm^2): interaction $F_{1,23}$=12.45, p=0.0018; H_2O non-stress (NS) vs TMT t_{23}=6.51, ##p<0.0001; EtOH NS vs TMT t_{23}=10.13, ##p<0.0001; TMT H_2O vs TMT EtOH t_{23}=3.92, **p=0.0041. Aqua bars are H_2O, red bars are EtOH. **D**, Pdyn-GFP quantification (mm^2): TMT main effect $F_{1,23}$=4.56, #p=0.0437. **E**, Colocalization between c-Fos and Pdyn-GFP (mm^2): interaction $F_{1,23}$=5.91, p=0.0233; EtOH NS vs TMT t_{23}=4.66, ##p=0.0007; TMT H_2O vs TMT EtOH t_{23}=3.65, **p=0.0081. **F**, Fiber photometry experimental design with Cre-inducible GCaMP7f in the BNST of Pdyn-Cre mice (n=3 H_2O, n=4 EtOH). **G**, Image of AAV-FLEX-GCaMP7f expression and fiber placement represented by a bracket. **H**, BNST^{PDYN} calcium transients (z-scores of Δf/f) after H_2O (aqua) and TMT (red) with inset average area under the curve (AUC) after DDW (squares) and TMT (circles). **I**, Percent change in AUC across 3 TMT exposures. EtOH TMT 1 vs TMT 3 t_3=3.35, *p=0.0441.

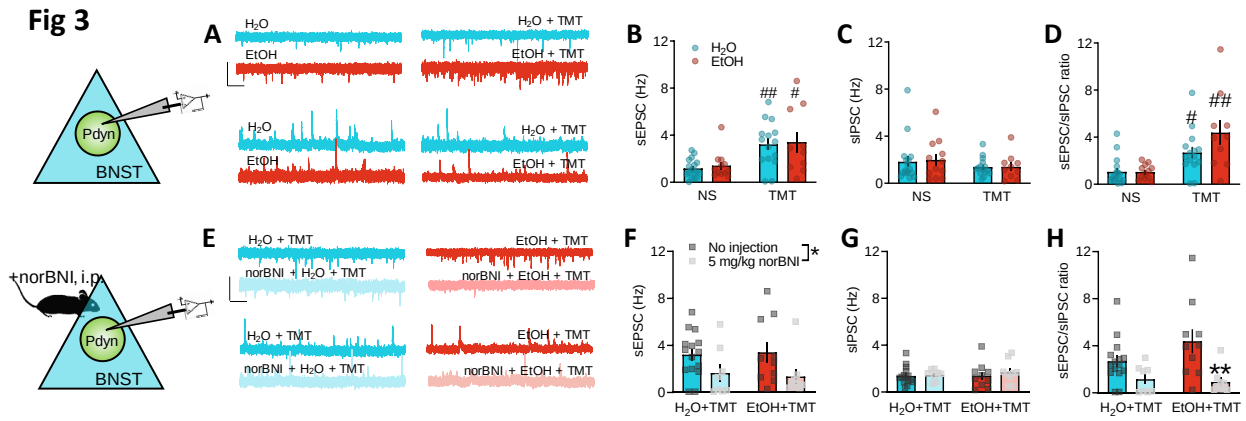

Fig 3. KOR regulation of increased synaptic transmission onto BNST Pdyn neurons after stress and EtOH. **A**, Representative traces of BNST^{PDYN} cell synaptic transmission in H_2O (n=6, 17 cells), EtOH (n=4, 12 cells), H_2O + TMT (n=5, 15 cells), and EtOH + TMT (n=4, 10 cells). Scale bar indicates 50 pA height and 1 sec time. **B**, Spontaneous excitatory post-synaptic currents (sEPSC) frequency (Hz): TMT main effect $F_{1,50}$=18.24, ##p<0.0001; H_2O NS vs TMT t_{50}=3.38, p=0.0028; EtOH NS vs TMT t_{50}=2.75, p=0.0167. **C**, Spontaneous inhibitory post-synaptic currents (sIPSC) frequency (Hz). **D**, sEPSC/sIPSC ratio: TMT main effect $F_{1,50}$=23.61, p<0.0001; H_2O NS vs TMT t_{50}=2.50, p=0.0312; EtOH NS vs TMT t_{50}=4.24, p=0.0002; TMT H_2O vs EtOH t_{50}=2.25, p=0.0566. **E**, Sample traces of BNST^{PDYN} cell synaptic transmission after 16 hr pretreatment with 5 mg/kg norBNI, i.p. Light aqua is norBNI + H_2O + TMT (n=3, 8 cells). Light red is norBNI + EtOH + TMT (n=3, 9 cells). Scale bar equals 50 pA height and 1 sec time. The non-injected H_2O + TMT and EtOH + TMT cells were used from panels B-D. **F**, sEPSC frequency (Hz): norBNI main effect $F_{1,38}$=6.96, *p=0.0120. **G**, sIPSC frequency (Hz). **H**, sEPSC/sIPSC ratio: norBNI main effect $F_{1,38}$=14.42, p=0.005; EtOH + TMT non-injected vs norBNI t_{38}=3.63, **p=0.0017.

Fig 4

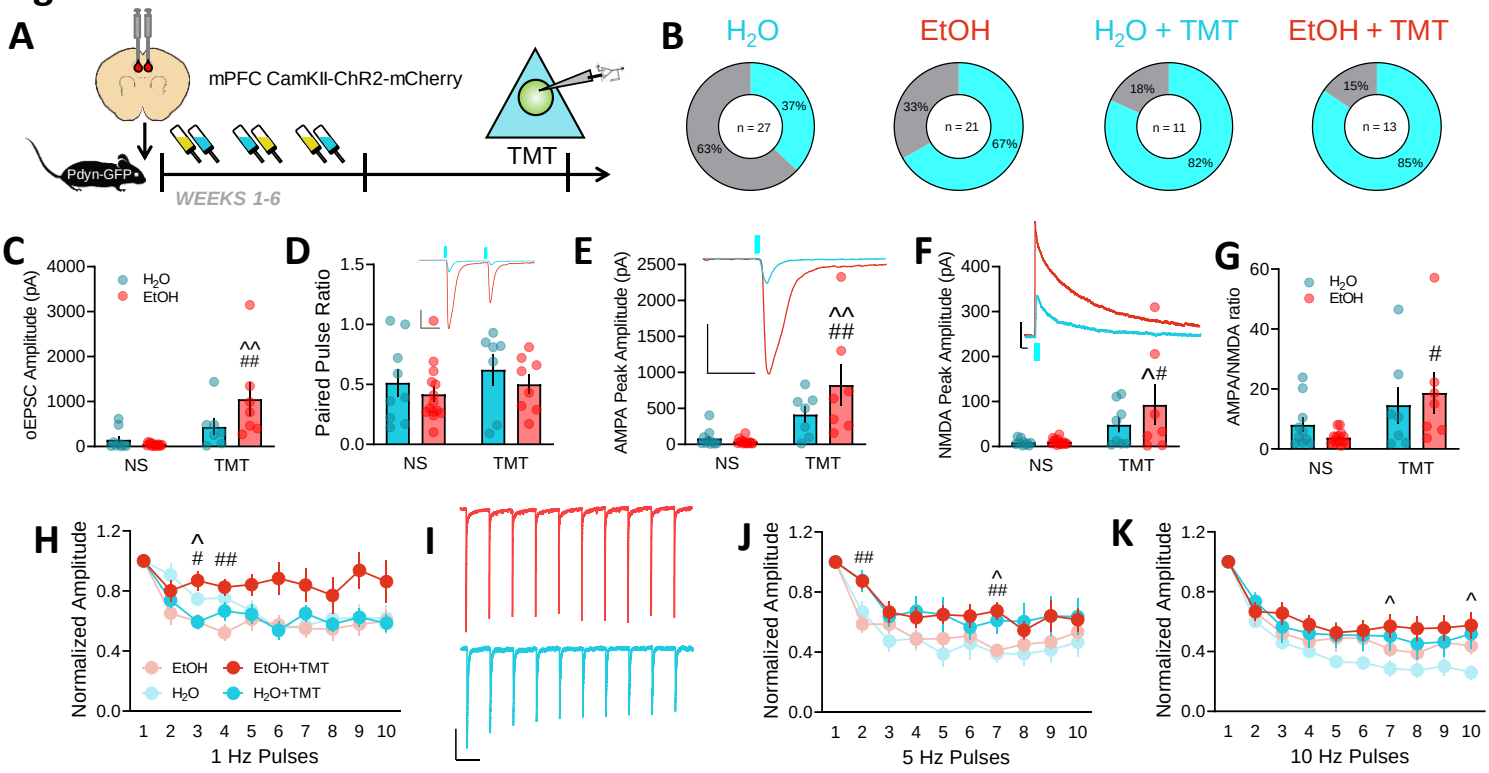

Fig 4. Cortical input onto BNST^{PDYN} cells gates stress-enhanced glutamatergic plasticity after history of alcohol. **A**, Experimental design testing synaptic connectivity of mPFC input to BNST^{PDYN} cells using channelrhodopsin (ChR2) after EtOH and TMT. **B**, Proportions of light-responsive (aqua) and non-light-responsive (grey) BNST^{PDYN} cells to optically-evoked EPSC in H_2O (10/27 responsive cells, n=7), EtOH (14/21 responsive cells, n=5), H_2O + TMT (9/11 responsive cells, n=4), and EtOH + TMT (11/13 responsive cells, n=4) groups: X^2_3=21.43, **p<0.0001. **C**, mPFC-BNST^{PDYN} oEPSC amplitude (pA): interaction $F_{1,33}$=4.74, *p=0.0367; H_2O non-stress (NS) vs EtOH + TMT t_{33}=3.70 ^^p=0.0047; EtOH NS vs EtOH + TMT t_{33}=4.50, ##p=0.0005. **D**, Paired pulse ratio. Inset example traces of H_2O + TMT (aqua) and EtOH + TMT (red) with blue LED onset. Scale bar indicates 200 pA height and 50 ms time. **E**, AMPA peak amplitude (pA): TMT main effect $F_{1,34}$=22.03, p<0.0001; H_2O NS vs EtOH + TMT t_{34}=4.28, ^^p=0.0009; EtOH NS vs EtOH + TMT t_{34}=4.82, ##p=0.0002. Inset AMPA traces of H_2O + TMT (aqua) and EtOH + TMT (red) with blue LED onset. Scale bar indicates 200 pA height and 50 ms time. **F**, NMDA peak amplitude (pA): TMT main effect $F_{1,34}$=12.09, p=0.0148; H_2O NS vs EtOH + TMT t_{34}=3.13, ^p=0.0213; EtOH NS vs EtOH + TMT t_{34}=3.27, #p=0.0148. Inset NMDA traces of H_2O +TMT (aqua) and IA+TMT (red) with blue LED onset. Scale bar indicates 200 pA height and 50 ms time. **G**, AMPA/NMDA ratio: TMT main effect $F_{1,34}$=8.12, p=0.0074; EtOH NS vs EtOH + TMT t_{34}=2.89, #p=0.0132. **H**, oEPSC normalized amplitude across 1 Hz pulse trains: interaction $F_{27,351}$=1.83, p=0.0080; Pulse 3: EtOH NS vs EtOH + TMT $t_{22.81}$=3.21, #p=0.0234; H_2O + TMT vs EtOH + TMT $t_{18.81}$=3.40, ^p=0.0180; Pulse 4: EtOH NS vs EtOH + TMT $t_{23.99}$=3.95, ##p=0.0036. **I**, Representative traces of 1 Hz pulse trains in EtOH + TMT (red) and H_2O + TMT (aqua) BNST^{PDYN} cells. Scale bar indicates 200 pA height and 1 sec time. **J**, oEPSC normalized amplitude across 5 Hz pulse trains: pulse main effect $F_{9,351}$=45.58, p<0.000; Pulse 2:

EtOH NS vs EtOH + TMT $t_{23.22}$=3.84, ##p=0.0049; Pulse 7: H_2O vs EtOH + TMT $t_{19.76}$=3.52, ^p=0.0131; EtOH NS vs EtOH + TMT $t_{21.66}$=3.67, ##p=0.0082. **K**, oEPSC normalized amplitude across 10 Hz pulse trains: pulse main effect $F_{9,342}$=69.96, p<0.0001; Pulse 7: H_2O vs EtOH + TMT $t_{19.59}$=2.94, ^p=0.0498; Pulse 10: H_2O vs EtOH + TMT $t_{18.14}$=3.05, ^p=0.0410.

Fig 1 Suppl 1

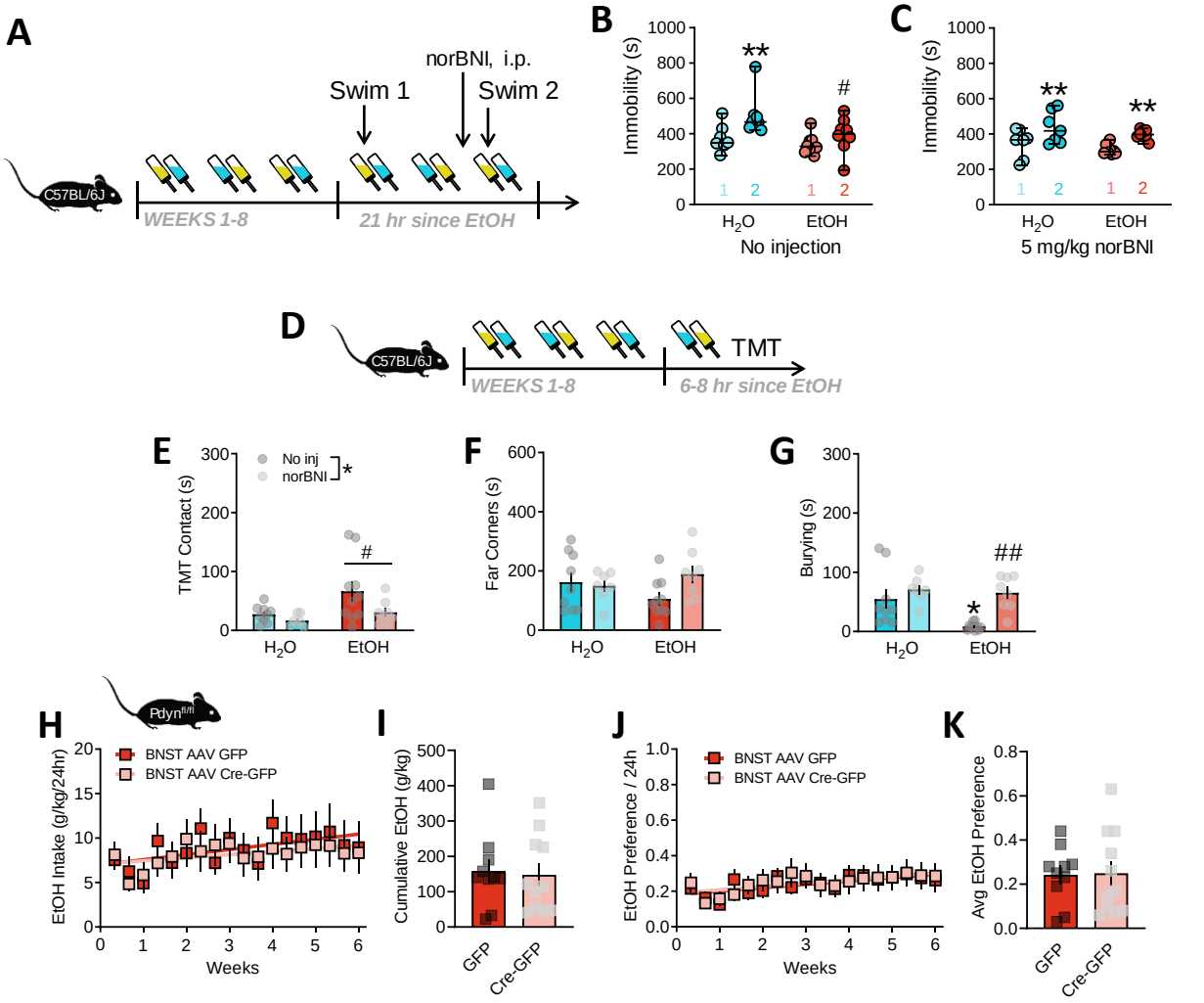

Fig 1 Suppl 1. A, Design of testing repeated forced swim behavior during acute withdrawal from EtOH (n=9) or H_2O controls (n=8). **B**, Immobility time (sec) during first (light aqua, light red) and second (aqua, red) forced swim tests in H_2O and EtOH mice. Main effect of Swim trial $F_{1,15}$=19.70, p=0.0005; H_2O Swim 1 vs Swim 2 t_{15}=4.29, **p=0.0013; Swim 2 H_2O vs EtOH t_{30}=2.63, #p=0.0266. **C**, Immobility time (sec) after 5 mg/kg norBNI injection before the second swim test in EtOH (n=8) and H_2O mice (n=7). Main effect of Swim trial $F_{1,13}$=36.60, p<0.0001; H_2O Swim 1 vs Swim 2 t_{13}=4.17, **p=0.0022; EtOH Swim 1 vs Swim 2 t_{13}=4.40, **p=0.0014. **D**, Schematic of TMT predator odor testing during acute withdrawal from EtOH (n=10) or H_2O controls (n=10) and norBNI-treated EtOH (n=7) and H_2O mice (n=8). **E**, TMT contact (sec): EtOH main effect $F_{1,30}$=4.26, #p=0.0479; norBNI main effect $F_{1,30}$=5.53, *p=0.0255. **F**, Far corners (sec). **G**, Burying (sec): EtOH main effect $F_{1,30}$=12.06, p=0.0016; H_2O no injection vs EtOH no injection t_{30}=3.28, *p=0.0156. NorBNI main effect $F_{1,30}$=5.95, p=0.0208. EtOH no injection vs norBNI t_{30}=3.93, ##p=0.0028. **H**, *Pdyn*$^{lox/lox}$ mice EtOH drinking (g/kg/24hr) across 6 wks with BNST GFP (red) or Cre-GFP (light red): Time main effect $F_{17,323}$=3.28, p=0.0095. **I**, Cumulative EtOH drinking (g/kg) per group: t_{19}=0.23, p=0.8181. **J**, *Pdyn*$^{lox/lox}$ mice daily EtOH preference across 6 wks with BNST GFP (red) or Cre-GFP (light red): Time main effect $F_{17,323}$=4.09, p=0.0019. **K**, Average EtOH preference per group: t_{19}=0.10, p=0.9221.

Fig 1 Suppl 2

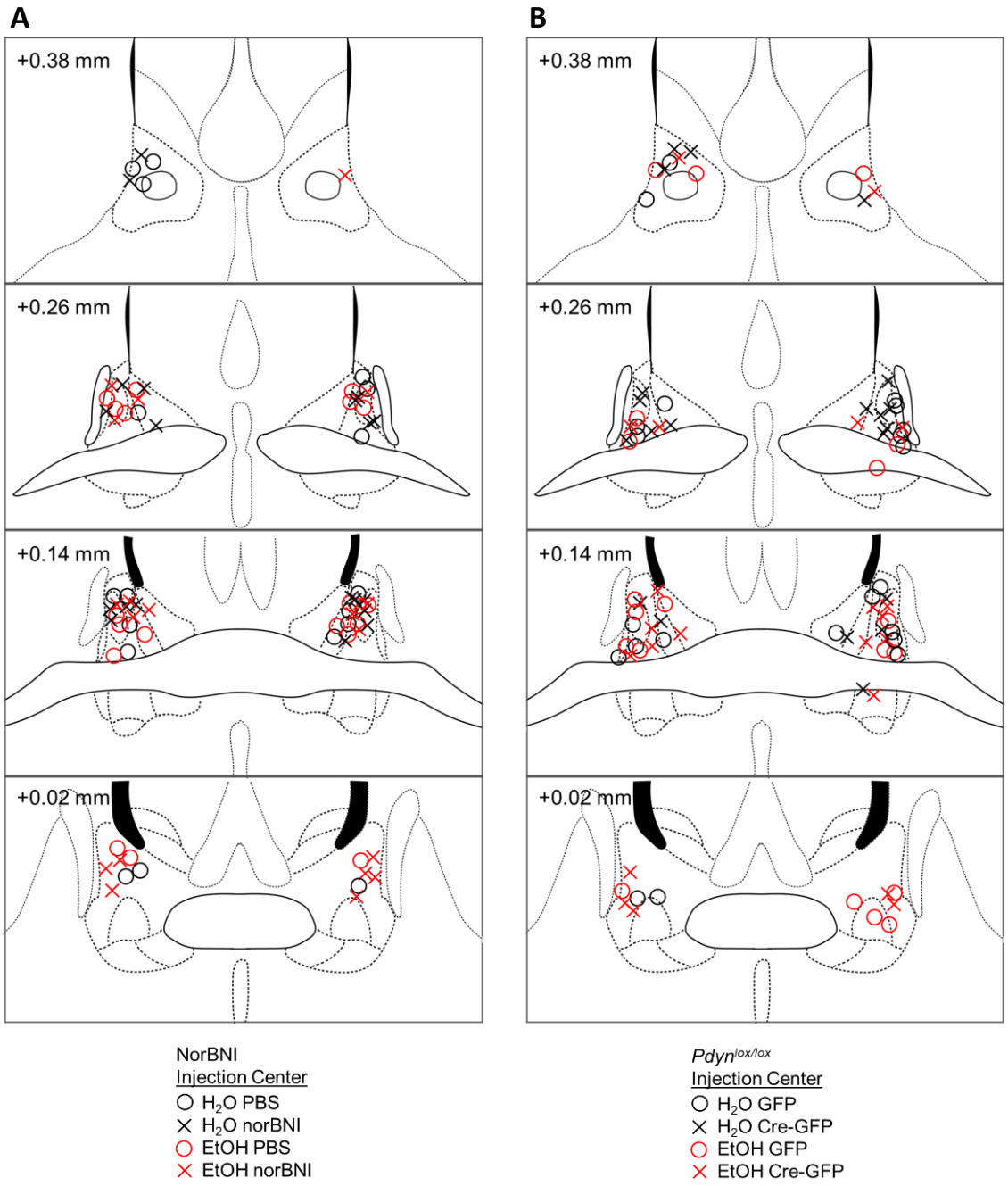

Fig 1 Suppl 2. Histological verification of stereotaxic injections in male mice. **A**, Correct placements of a single norBNI or PBS infusion are shown in coronal sections in millimeters from bregma surrounding the BNST of C57BL/6J mice. Circles represent the injection center of PBS, and crosses represent norBNI. Both groups had 10ul GFP to mark the injection site. **B**, Correct BNST placements of AAV-Cre-GFP or AAV-GFP infusion are shown in coronal sections in millimeters from bregma in a floxed Pdyn mouse line. Injection centers are represented by circles for GFP or crosses for Cre-GFP.

Fig 2 Suppl 1

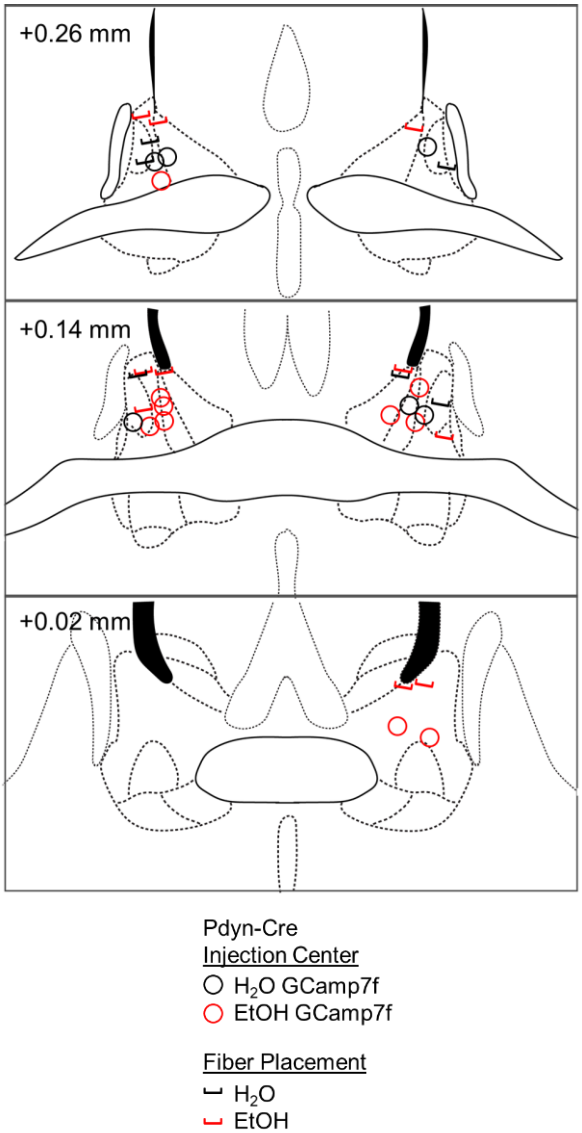

Fig 2 Suppl 1. Histological verification of stereotaxic injection and fiber placement in Pdyn-Cre mice. Correct placements of AAV-FLEX-GCaMP7f bilateral infusion and fiber placements are shown in coronal sections in millimeters from bregma surrounding the BNST in Pdyn-Cre mice. Circles represent injection center, and bracket represents fiber placement.

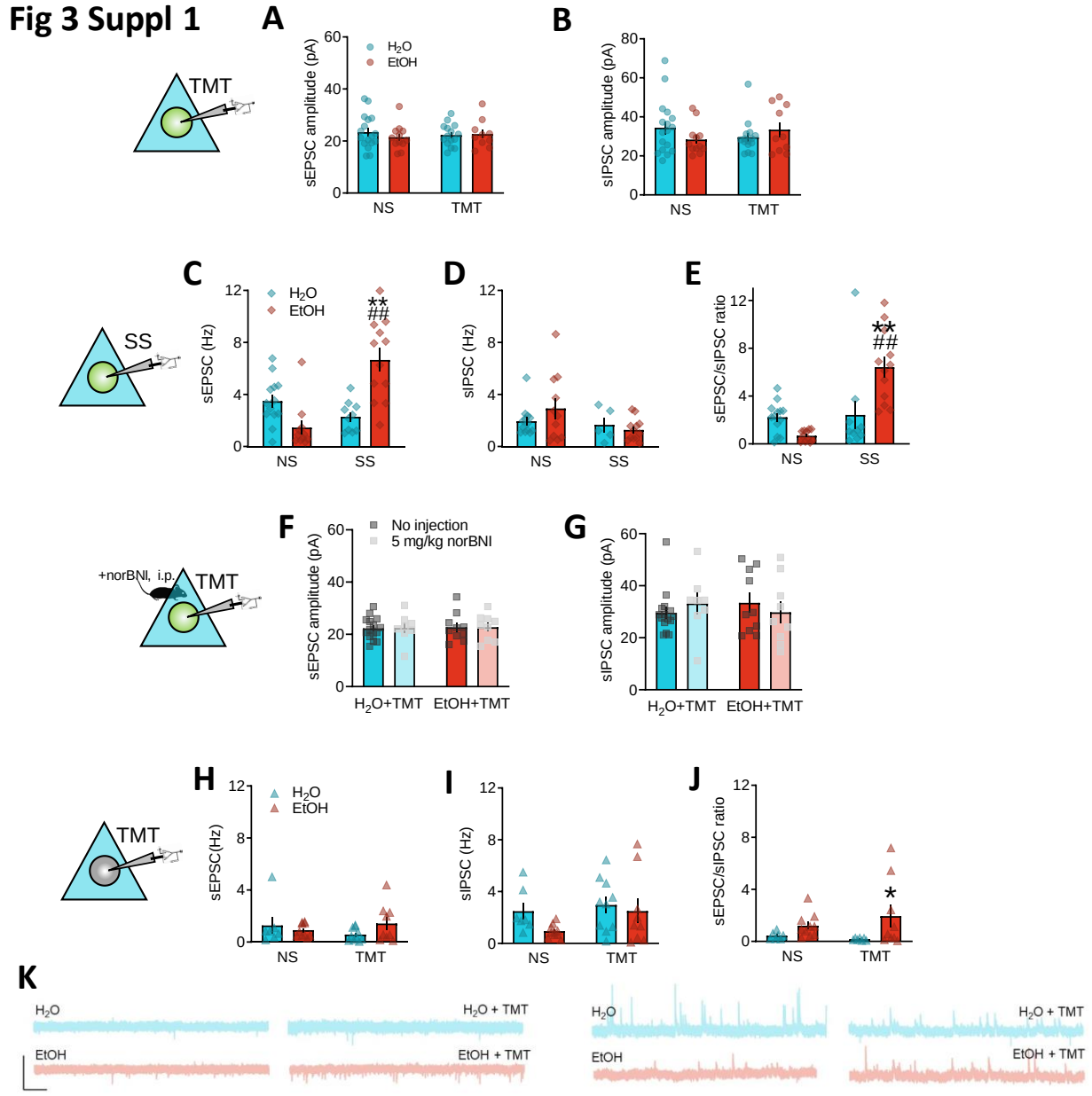

Fig 3 Suppl 1. A, TMT BNST^{PDYN} cell synaptic transmission sEPSC amplitude (pA). **B**, sIPSC amplitude (pA). **C**, Swim stress (SS) BNST^{PDYN} cell sEPSC frequency (Hz; H_2O n=4, 13 cells; EtOH n=3, 11 cells; H_2O + SS n=3, 10 cells; EtOH + SS n=4, 12 cells): interaction $F_{1,42}$=26.07, p<0.001; H_2O + SS vs EtOH + SS t_{42}=4.82, **p=0.0001; EtOH NS vs SS t_{42}=5.89, ##p<0.0001. **D**, sIPSC frequency (Hz). **E**, sEPSC/sIPSC ratio: interaction $F_{1,42}$=14.79, p=0.0004; H_2O + SS vs EtOH + SS t_{42}=3.84, **p=0.0004; EtOH NS vs SS t_{42}=5.65, ##p<0.0001. **F**, NorBNI pretreatment BNST^{PDYN} cell sEPSC amplitude (pA). **G**, sIPSC amplitude (pA). **H**, BNST non-GFP-labeled cell synaptic transmission sEPSC frequency (Hz; H_2O n=3, 7 cells; EtOH n=3, 10 cells; H_2O + TMT n=3, 10 cells; EtOH + TMT n=3, 9 cells). **I**, sIPSC frequency (Hz). **J**, sEPSC/sIPSC ratio: EtOH main effect $F_{1,32}$=7.12, p=0.0119; TMT H_2O vs TMT EtOH t_{32}=2.70, *p=0.0216. **K**, Representative traces of BNST non-GFP cells. Scale bar indicates 50 pA height and 1 sec time.

Fig 4 Suppl 1

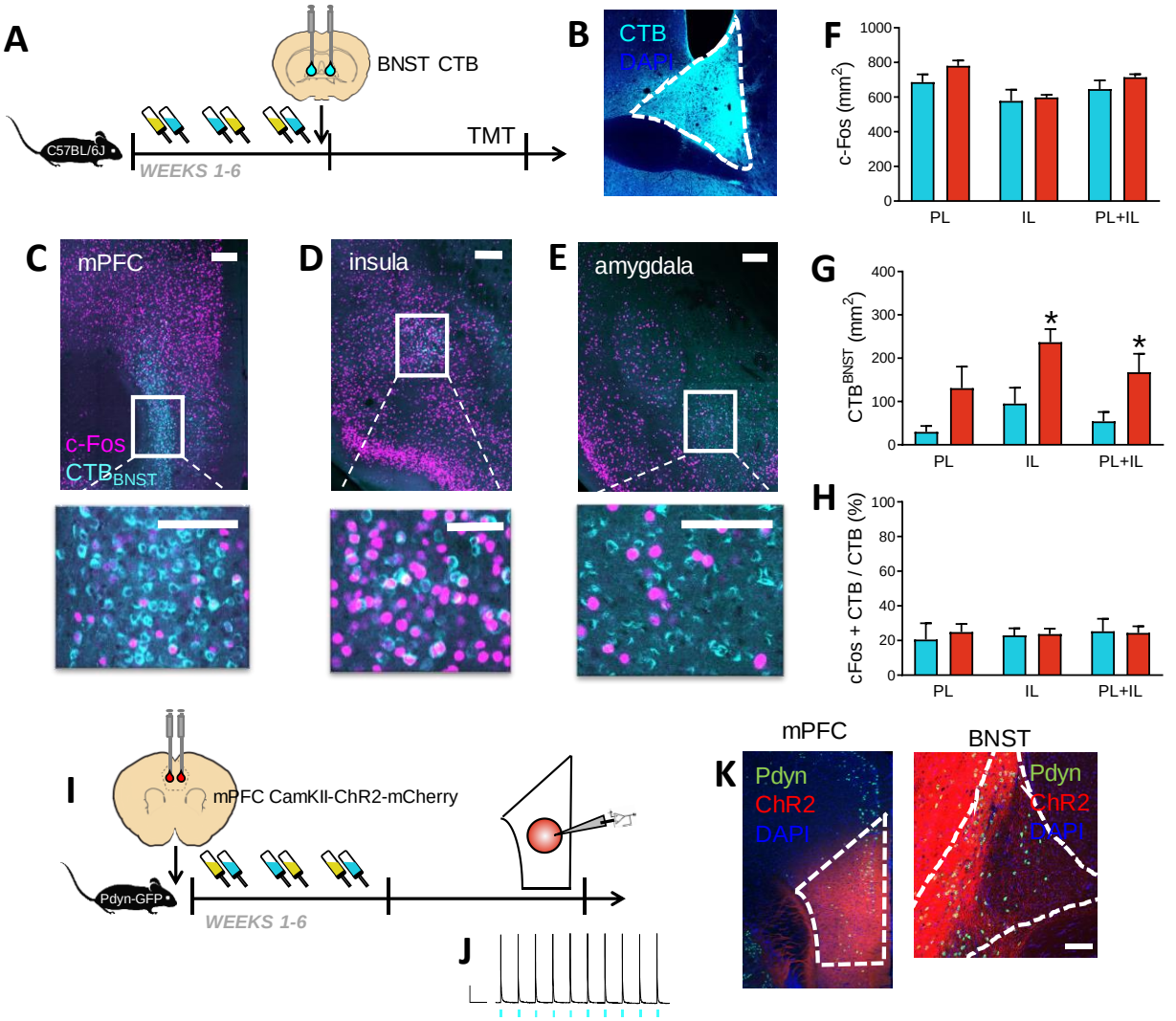

Fig 4 Suppl 1. A, Schematic of choleratoxin B (CTB) retrograde tracing in BNST before TMT and c-Fos immunohistochemistry. **B**, Image of CTB injection into the BNST. c-Fos immunostaining (pseudocolored purple) and CTB 555 from the BNST (pseudocolored aqua) in the **C**, medial prefrontal cortex (mPFC), **D**, insula, **E**, amygdala. Scale bars measure 200 µm. Inset photo scale bars measure 100 µm. **F**, mPFC c-Fos quantification (mm^2) in prelimbic (PL), infralimbic (IL), and combined PL+IL. Aqua bars are H_2O (n=3), red bars are EtOH (n=4). **G**, CTB quantification from the BNST: IL H_2O vs EtOH t_5=2.82, *p=0.0369; PL+IL H_2O vs EtOH t_5=2.58, *p=.0496. **H**, Percentage of colocalization of c-Fos and CTB over total CTB (%). **I**, Design of synaptic strength physiology experiments from mPFC to BNST^{PDYN} cells. **J**, Representative traces of optically-evoked mPFC action potentials at 1 Hz. Blue rectangles indicate 470nm LED onset. Scale bar indicates 20 mV and 1 sec. **K**, Image of CamKII-ChR2-mCherry expression in the mPFC (left) and at BNST terminals (right). Pdyn-GFP cells are green. Inset photo scale bars measure 100 µm.